sustainability

MDPI

Article

Simulation and Machine Learning Investigation on Thermoregulation Performance of Phase Change Walls

Xin Xiao [1,2,*], Qian Hu [1], Huansong Jiao [1], Yunfeng Wang [2] and Ali Badiei [3,*]

[1] College of Environmental Science and Engineering, Donghua University, Shanghai 201620, China; 2222366@mail.dhu.edu.cn (Q.H.); 2212195@mail.dhu.edu.cn (H.J.)
[2] Yunnan Provincial Rural Energy Engineering Key Laboratory, Kunming 650550, China; wangyf@ynnu.edu.cn
[3] School of Engineering, University of Central Lancashire, Preston PR1 2HE, UK
* Correspondence: xin.xiao@dhu.edu.cn (X.X.); abadiei@uclan.ac.uk (A.B.); Tel.: +86-(0)-1896-4749723 (X.X.); +44-(0)-1772-894499 (A.B.)

Abstract: The outdoor thermal environment can be regarded as a significant factor influencing indoor thermal conditions. The application of phase change materials (PCMs) to the building envelope has the potential to improve the heat storage performance of building walls and, therefore, effectively regulate the temperature variations of the inner surfaces of walls. COMSOL Multiphysics software was adopted firstly to perform the simulations on the thermoregulation performance of phase change wall; the time duration of the temperature at the internal side maintained within the thermal comfort range was used as a quantitative evaluation index of the thermoregulation effects. It was revealed from the simulation results that the time durations of thermal comfort were extended to 5021 s and 4102 s, respectively, when the brick walls were filled with two types of composite PCMs, namely eutectic hydrate (EHS, $Na_2CO_3{\cdot}10H_2O$ and $Na_2HPO_4{\cdot}12H_2O$ with the ratio of 4:6)/5 wt.% BN and EHS/5 wt.% BN/7.5 wt.% expanded graphite (EG), under the conditions of 18 °C ambient temperature and 60 °C heating temperature at the charging stage. Both of them were longer than 3011 s, which corresponds to a pure brick wall. EHS/5 wt.% BN/7.5 wt.% EG exhibited better leakage prevention performance and, therefore, was a candidate for actual application, in comparison with EHS/5 wt.% BN. Then, a machine learning training process focused on the temperature control effects of phase change wall was carried out using a BP neural network, where the heating surface and ambient temperature were used as input variables and the time duration of indoor thermal comfort was the output variable. Finally, the learning deviation between the raw data and the results obtained from machine learning was within 5%, indicating that machine learning can accurately predict the temperature control effects of the phase change wall. The results of the simulations and machine learning can provide information and guidance for the advantages and potentials of PCMs of hydrate salts when being applied to the building envelope. In addition, the accurate prediction of machine learning demonstrated its application prospects to the research of phase change walls.

Keywords: phase change wall; radiative heating; numerical simulation; machine learning

Citation: Xiao, X.; Hu, Q.; Jiao, H.; Wang, Y.; Badiei, A. Simulation and Machine Learning Investigation on Thermoregulation Performance of Phase Change Walls. *Sustainability* **2023**, *15*, 11365. https://doi.org/10.3390/su151411365

Academic Editor: Antonio Caggiano

Received: 22 June 2023
Revised: 15 July 2023
Accepted: 17 July 2023
Published: 21 July 2023

1. Introduction

Outdoor climate conditions tend to influence the indoor thermal environment to a great extent. The application of phase change walls to building enclosures has great prospects to improve effectively the indoor thermal environment and reduce the energy consumption generated by heating and cooling and, thus, makes contributions to providing better thermal comfort conditions for humans. In view of the large costs in time and some restrictions in construction of the actual building, numerical simulation is one type of research method that has received much attention and is intended to supply guidance for practical application [1]. At present, many researchers place much emphasis on the influences of the thermophysical properties, contents, and positions of phase change materials (PCMs) and their combination with building materials. Additionally emphasized

are the climate conditions on the heat transfer characteristics of phase change walls and indoor air temperature and the energy consumption based on the corresponding mathematical models. The associated indexes can be adopted to describe specific influence effects, which usually include the efficiency of the PCM coverage, temperature time lag, temperature decrement factor, and the energy demand and energy saving rate. Javidan et al. [2] conducted numerical simulations on paraffin phase change walls to study the melting characteristics when different constant heat fluxes were imposed respectively, and it was revealed that the larger heat flux corresponded to the quicker melting rate and more evident buoyancy effects. In addition, the delay effects of the heat transferred from the external side to the internal side became more significant as the thickness of the phase change layer increased. Li et al. [3] established the heat transfer model of a phase change mortar wall whose thermophysical properties were determined by a mesoscopic model to discuss the variations of heat transfer characteristics brought by differences in the concentrations, phase change temperatures, and latent heats of the PCMs. It was demonstrated that the phase change wall contributed to reducing the fluctuation of indoor temperature in transition seasons and to decreasing the summer building energy consumption effectively in terms of the climate conditions of hot summer and cold winter regions. Ye et al. [4] compared different influencing factors on the temperature variations and energy saving effects based on the phase change building enclosure model with the mixture of $CaCl_2 \cdot 6H_2O$ and expanded graphite (EG) as the PCM and concluded that the density and thermal conductivity of the PCM failed to influence greatly the thermophysical properties of the building enclosure, while the thickness of the PCM layer, the building orientation, and the local climate were significant factors for the phase change process of the PCM. Derradji et al. [5] adopted numerical simulations to study the positive effects of the office model incorporating PCMs, and the simulation results suggested that indoor temperatures in the winter and summer could be increased by approximately 3 °C and reduced by 7 °C, respectively. Charvátová et al. [6] applied PCMs to a wooden house model to study the changes of temperature with the time of indoor air and the temperature distribution of the building enclosure after the addition of the PCM, and the simulation results revealed that, in comparison with the building model with PCMs positioned in the ceiling and walls, the wall opposite the window side covered by the PCM at the internal side was more advantageous in decreasing the indoor temperature, where the maximum reduction reached 31.1%. Ye et al. [7] laid the composite PCMs of $CaCl_2 \cdot 6H_2O$-$Mg(NO_3)_2 \cdot 6H_2O$/EG at the roof and south wall, respectively, the melting temperature and latent heat of which could vary with the increase in the ratio of two hydrate salts, to determine the appropriate melting temperature of the PCM and the position of the PCM layer for an evident decrease in energy demand in different climate regions based on the simulation results of various cases. It was advised that a PCM layer positioned at the internal side always corresponded to low energy demand, and the melting temperature of the PCM required to obtain a large reduction in energy demand would change in different areas. Zhu et al. [8] simulated the application of double-layer Trombe phase change walls in a building enclosure on the basis of the Wuhan climate, and it was found that peak cold and heat loads of the building were lowered by 9% and 15%, respectively, compared with that of the Trombe wall without PCMs. Rehman et al. [9] carried out numerical simulations on double-layer phase change walls with two types of PCMs at the melting temperatures of 29 °C and 13 °C to improve thermal comfort conditions and reduce energy consumption both in cold and hot weather conditions. Gopinath et al. [10] studied the heat storage performances of phase change walls packed with PCMs of $CaCl_2 \cdot 6H_2O$, n-octadecane, and $Na_2CO_3 \cdot 10H_2O$, respectively, and concluded that indoor temperatures at 12 p.m. could be reduced by 4~5 °C. Kant et al. [11] investigated the influences of the position and thickness of the PCM layer as well as the phase change temperature of the PCMs on the heat transfer characteristics of the phase change walls by numerical simulations, and it was found that when a PCM layer with a wide thickness was laid in the middle side and its melting temperature was close to the indoor air temperature, the heat transfer from outdoors to indoors could be lowered.

Govindasamy and Panwar [12] adopted palm fat as bio-PCM and discussed the effects of the thickness of the PCM layer on the thermal comfort performance in buildings and, on the basis of simulation data, pointed out that the temperature fluctuation of the inner surface of the phase change wall, especially within the scope of 2 p.m.~10 p.m., could be evidently reduced by the increase in the PCM layer. Rai [13] simulated the variations of building peak loads caused by different positions of the PCM layer and insulation layer, which were found to be greatly decreased when the phase change temperature of the PCM layer was near or slightly higher than the indoor temperature and was arranged at the internal side, with the insulation layer at the external side. Zhang et al. [14] investigated the new-type phase change walls, whose PCMs would reverse position with the insulation material. In daytime, it was close to the external side and could absorb the heat transferred from the outdoors to the walls in the winter, while the position of the PCM after sunset would be close to the internal side; therefore, heat was released indoors in a timely manner, which allowed the time duration of the indoor temperature to be maintained within the extended thermal comfort range compared with that of traditional phase change walls. Mi et al. [15] compared the energy saving effects and economic benefits of a building model containing PCMs in five climate zones in China by simulation and concluded that the application of phase change walls in the hot summer and cold winter regions achieved the optimal energy conservation effects and corresponded to higher economic values. Qu et al. [16] analyzed different influences of four factors—building type, layout position of PCM layer, PCM type, and PCM thickness—on extending the thermal comfort time and reducing the electricity consumption based on multi-factor orthogonal simulations, whose results indicated that the building type was the more critical parameter, while the variation of the PCM thickness corresponded to a lesser influence. Wang et al. [17] proposed applying the PCM with variable optical characteristics in building roofs to achieve energy saving effects by changing the solar energy absorption in different seasons. Abd El-Raheim et al. [18] integrated various PCMs with different melting temperatures at different layout positions and wall orientations into a heavy-structure building envelope to compare the positive roles of the reduction in hours not within thermal comfort conditions or cooling demand in hot regions.

In addition to numerical simulations, machine learning can also be considered as an efficient research method, which not only avoids much time and material costs but has great advantages and prospects in terms of reliable analysis on abundant data and their inherent relationships [19]. At present, machine learning has been widely applied in the field of energy saving in buildings [20,21]. Bacher et al. [22] adopted machine learning to predict the heat loads of 16 houses in Denmark based on the least squares time series model, which could output the results of heat loads per hour, with a maximum of 42 h in advance. Idowu et al. [23] investigated 10 buildings in Sweden, including houses and commercial structures, as the study subjects and employed different machine learning methods to predict the heat loads. It was suggested that the method of support vector machine returned the best prediction effects and could restrict the deviation to within 7%. Al-Shammari et al. [24] optimized the algorithms for the prediction of building heat load based on support vector machine, and the obtained results were then compared with other ones corresponding to the artificial neural network, genetic algorithm, and original support vector machine models. It was concluded that the model after optimization had better prediction accuracy. Jovanović et al. [25] made predictions on the heating consumption of a university campus via three types of artificial neural network models, including feed forward backpropagation neural network, radial basis function network, and adaptive neuro-fuzzy interference system, involving various input variables, such as mean daily outside temperature and heating consumption of the previous day. It was advised that the ensemble of neural networks corresponded to more accurate prediction results in comparison with that of a single model due to the better fitting effects and lower error between measured heating consumption and predicted consumption. In addition to the studies on the building loads [26] and building energy consumption [27], machine learning is also viewed as an effective way

to research the associated contents of the PCMs incorporated into the building envelope. Bhamare et al. [28] adopted different models based on machine learning and deep learning to predict the thermal performance of PCMs contained in building roofs with the variation of thermophysical properties and concluded that the gradient boosting regression model and artificial neural network model presented higher prediction accuracy according to the evaluation index of the measure of key responses. Alnaqi et al. [29] combined the use of PCMs in the building envelope and extra convection to lower the energy demand and conducted studies on the heat transfer of the phase change walls and phase change roof based on a neural network, the calculation results of which showed good agreement with the numerical data, where the corresponding coefficients of determination reached 0.991 and 0.979, respectively. Urresti et al. [30] applied the artificial neural network to analyze the thermal behavior of PCMs integrated in the building envelope and discussed the heat flux with the variation of time. The training results of machine learning were close to those of the simulation data, and the mean squared error (MSE) was only 0.0584 W/m^2, which was lower than the accuracy error. However, the model after training had worse generalization when data different from the training data were input.

Based on the above research of simulation and machine learning regarding the phase change walls, most of the PCMs were organic ones or single inorganic hydrate salt, and the physical properties of the PCMs were sourced from simulation software in other cases. In addition, the PCMs were usually incorporated into the building walls in the form of panel or direct mixing with the building materials. Additionally, there is relatively little research focused on the application of machine learning to study phase change building walls. In the present study, the topic is focused on studying the thermoregulation performances of phase change brick walls at the inner face under different ambient conditions via simulations and machine learning. The accuracy of the simulated models and relevant settings was verified firstly by comparing the simulation results and experimental data at the same ambient and heating temperatures. Then, other simulations under different ambient temperatures and heating temperatures were conducted to research their effects on extending the time duration within the thermal comfort range. Finally, the series simulation results were applied to machine learning to predict the thermoregulation effects of the phase change walls under unknown conditions after demonstrating the accuracy of the machine learning model. The PCMs we used were binary eutectic hydrate salts of $Na_2CO_3{\cdot}10H_2O$ and $Na_2HPO_4{\cdot}12H_2O$ added with BN or EG, which not only avoided the safety issues caused by organic PCMs but also allowed the retrieval of the supercooling and phase separation phenomena of single hydrate salt. Moreover, the phase change building wall in this work is structured by hollow bricks where PCMs are filled into the holes, which makes contributions to weakening the negative effects of the melting process, such as leakage coupled with EG. Additionally, the investigations on the influence of PCMs on lowering the temperature of the phase change wall at the internal side under different environmental conditions are significant since the reduction would influence the radiation heat transfer between the walls and humans and, therefore, improve the indoor thermal comfort to different extents in the summer.

2. Numerical Simulations

The models of the pure brick wall and the brick walls filled with composite PCMs were established with COMSOL Multiphysics 6.0, so as to further study the improvements in the thermoregulation performance of the phase change walls compared with the pure brick wall under various environmental conditions. In addition, the overall temperature distributions of the walls could be intuitively observed. Additionally, the simulation results provided more raw data for machine learning, which was beneficial for the enhancement of the training and prediction effects. In the present study, two types of PCMs were involved: EHS/5 wt.% BN and EHS/5 wt.% BN/7.5 wt.% EG, both of which possess appropriate melting temperatures within the thermal comfort range of 22~28 °C [31]. EHS denotes the mixture of $Na_2CO_3{\cdot}10H_2O$ and $Na_2HPO_4{\cdot}12H_2O$ with the ratio of 4:6; both $Na_2CO_3{\cdot}10H_2O$

and $Na_2HPO_4 \cdot 12H_2O$ belong to inorganic hydrate salts and, therefore, avoid the potential safety issues brought by organic PCMs, such as flammability and toxicity. Moreover, the two types of hydrate salts possess high charging/discharging efficiencies and economic benefits due to their large latent heat values and low costs in comparison with organic PCMs and other hydrate salts. EHS was prepared by mixing $Na_2CO_3 \cdot 10H_2O$ and $Na_2HPO_4 \cdot 12H_2O$ to regulate the melting temperature within the thermal comfort temperature range and to eliminate the phase separation phenomenon. The addition of BN was beneficial for decreasing the subcooling degree of EHS, while EG could make contributions to enhancing the thermal conductivity and preventing the leakage of PCMs caused by melting. However, the existence of EG caused the latent heat to be reduced. The specific values of melting temperature and latent heat for the two types of PCMs are summarized in Table 1, which were presented in a previous study [32].

Table 1. Melting temperatures and latent heat values of composite PCMs [32].

PCMs	Melting Temperature (°C)	Latent Heat (kJ/kg)
EHS/5 wt.% BN	25.49	196.85
EHS/5 wt.% BN/7.5 wt.% EG	25.99	171.63

2.1. Geometric Models

The models of the pure brick wall and brick wall filled with composite PCMs were structured by eight bricks with the size of 200 mm × 50 mm × 50 mm, and the cement with the thickness of 10 mm was paved on the upper side of the bricks and the combination positions of the bricks; thus, the two models on the whole presented the size of 410 mm × 50 mm × 240 mm. The simulated models were consistent with the experimental walls in terms of structure and size [32], which are shown in Figure 1(a-I,a-II); the models after meshing are shown in Figure 1(b-I,b-II).

The front and rear sides of the models represented the indoor and outdoor sides, respectively. Four temperature probes were arranged in the middle of the bricks' surface of the second and third layers at the internal side so that the temperature corresponding to internal side could be calculated, which equaled the average of the four monitored temperatures.

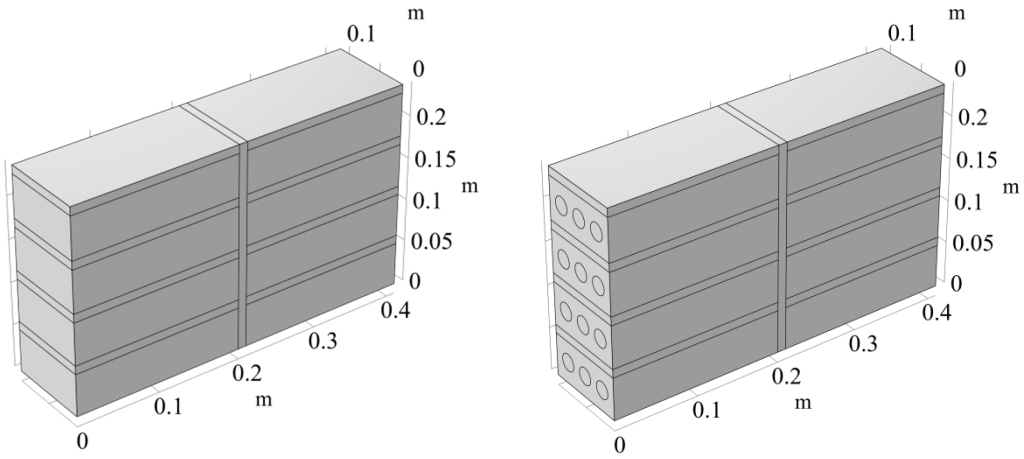

(a-I) **(a-II)**

Figure 1. *Cont.*

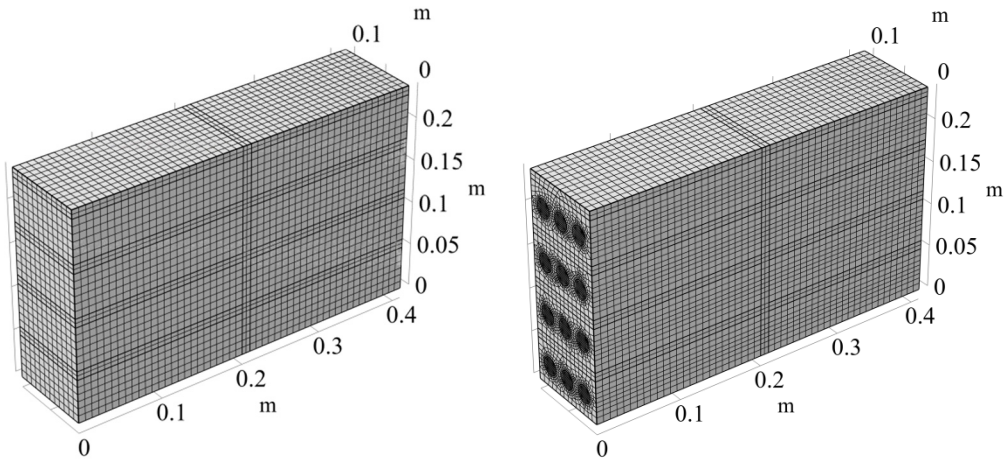

Figure 1. Schematic diagram of different walls before and after meshing: (**a-I**) pure brick wall before meshing; (**a-II**) brick wall filled with PCMs before meshing; (**b-I**) pure brick wall after meshing; (**b-II**) brick wall filled with PCMs after meshing.

Furthermore, some assumptions were made regarding the models in the simulations for simplification:

(1) The contact between the bricks and cement or the PCMs formed a good fit; therefore, the thermal contact resistance between them could be disregarded;
(2) The PCMs and bricks were distributed evenly and possessed isotropy characteristics in terms of physical properties, such as thermal conductivity. In addition, the variations in volume for the PCMs during the phase change process were disregarded;
(3) The phase changes of the PCMs were characterized by the enthalpy method; thus, tracking the position of the solid–liquid interface in the phase change process could be avoided, and the internal convection was not taken into account due to the small size of the holes in the bricks.

2.2. Solution of the Models

2.2.1. Governing Equation

The energy equation involved in the simulation is shown as follows:

$$\rho c_{\mathrm{p}} \frac{\partial T}{\partial t} = \nabla \cdot (k \nabla T) \tag{1}$$

where T (K), ρ (kg/m^3), c_{p} (J/(kg·K)), and k (W/(m·K)) refer to temperature, density, specific heat capacity, and thermal conductivity, respectively.

2.2.2. Boundary Conditions

The temperature of the outer surface of the mathematical model was known, whose values with the variation of time were obtained from the experimental results measured by thermocouples and then input as the partial boundary conditions to perform the simulation. Considering the mathematical model of the phase change brick wall filled with EHS/5 wt.% BN/7.5 wt.% EG as an example, the specific temperature variation profiles of the outer surface under the three heating temperatures of 50 °C, 55 °C, and 60 °C are shown in Figure 2 [32]. In addition, the bottom of the mathematical model was the adiabatic surface, and the remainder of the surfaces, including the upper and inner surfaces as well as two sides, were set as natural convection heat transfer with ambient air. The temperature of these surfaces was 18 °C, and the coefficients of convection heat transfer at the upper horizontal face and vertical faces, including the inner face and two sides, were calculated

based on the Equations (2) and (3), both of which were sourced from COMSOL Multiphysics software 6.0.

$$h_1 = \begin{cases} \frac{k}{L}0.54Ra_L^{1/4} & \text{if } T > T_{ext} \text{ and } 10^4 \le Ra_L \le 10^7 \\ \frac{k}{L}0.15Ra_L^{1/3} & \text{if } T > T_{ext} \text{ and } 10^7 \le Ra_L \le 10^{11} \\ \frac{k}{L}0.27Ra_L^{1/4} & \text{if } T \le T_{ext} \text{ and } 10^5 \le Ra_L \le 10^{10} \end{cases} \quad (2)$$

where h_1 is the convection heat transfer coefficient at the horizontal face, (W/(m^2·K)); L denotes characteristic length, (m); and Ra_L stands for Rayleigh number, the expression of which is shown in Formula (4).

$$h_2 = \begin{cases} \frac{k}{L}\left(0.68 + \frac{0.67Ra_L^{\frac{1}{4}}}{\left(1+\left(\frac{0.492k}{\mu c_p}\right)^{\frac{9}{16}}\right)^{\frac{4}{9}}}\right) & Ra_L \le 10^9 \\ \frac{k}{L}\left(0.825 + \frac{0.387Ra_L^{\frac{1}{6}}}{\left(1+\left(\frac{0.492k}{\mu c_p}\right)^{\frac{9}{16}}\right)^{\frac{8}{27}}}\right)^2 & Ra_L > 10^9 \end{cases} \quad (3)$$

where h_2 is the convection heat transfer coefficient at the vertical face, (W/(m^2·K)); μ means dynamic viscosity, (Pa·s).

$$Ra_L = GrPr = \frac{\rho^2 g \alpha c_p \Delta T L^3}{\mu k} \quad (4)$$

where Gr and Pr are the Grashof number and Prandt number, respectively; g is the gravitational acceleration, (m·s^2); α is the volume expansion coefficient of the air, (1/K); and ΔT is the temperature difference between the inner face of the wall and the air, (K).

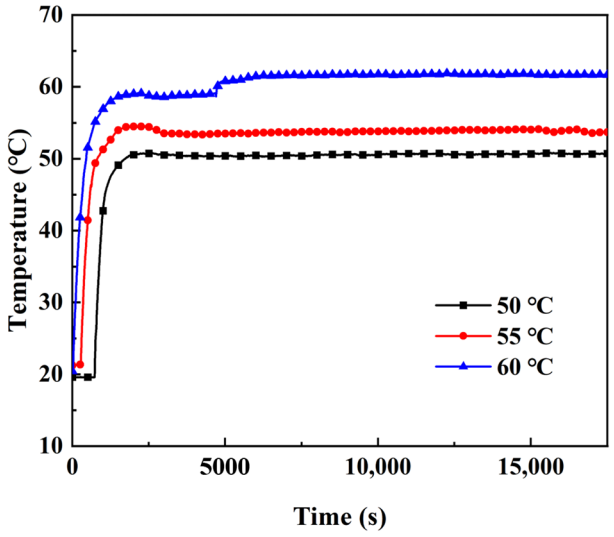

Figure 2. Temperature variation profiles of outer surfaces for brick wall filled with EHS/5 wt.% BN/7.5 wt.% EG under different heating temperatures [32].

2.2.3. Initial Conditions

The initial temperature of the entire mathematical model remained the same as that in the experimental measurements. Due to the influence of the local climate, there existed a temperature fluctuation of the indoor air in spite of the temperature being regulated at 18 °C by the air conditioning equipment; thus, the initial temperature of the brick models in the simulations exhibited changes.

2.2.4. Physical Properties of Materials and Initial Values

The associated parameters of thermal conductivity, specific heat capacity, and density were required to describe the thermodynamic properties of the materials involved in the simulations. The specific values of the cement, brick, EHS/5 wt.% BN, and EHS/5 wt.% BN/7.5 wt.% EG are summarized in Table 2 [32]. In terms of the specific heat capacity, a differential scanning calorimeter (DSC) was used to conduct the measurements. It can be seen from Figure 3 that the specific heat capacity of the brick in the range of 10~70 °C had little changes and was, therefore, viewed as a constant of 3040 J/(kg·K) in the simulations, which was the mean value in the above-mentioned temperature range. By contrast, obvious peaks appeared in the specific heat capacities curves of EHS/5 wt.% BN and EHS/5 wt.% BN/7.5 wt.% EG around the phase change temperature; thus, the corresponding specific heat capacities with the changes of temperature were input as the form of the interpolation function. Based on the enthalpy method, the phase change process of the PCMs in the bricks could be presented by the specific heat capacity.

Table 2. Physical properties of various materials [32].

Materials	Thermal Conductivity (W/(m·K))	Specific Heat Capacity (J/(kg·K))	Density (kg/m^3)
Cement	0.93	1050	1800
Brick	1.209	3040	2240
EHS/5 wt.% BN	0.917	Interpolation method	1380
EHS/5 wt.% BN/7.5 wt.% EG	2.360	Interpolation method	1420

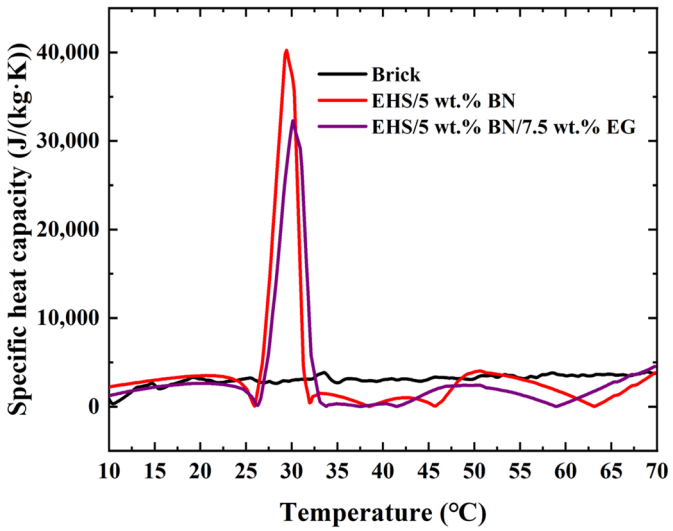

Figure 3. Specific heat capacity curves of different materials [32].

2.2.5. Validated Experiments

As mentioned above, the temperatures of the surface representing the outdoor side in simulations were determined by the experiments. The experimental apparatus illustrated in the previous study [32] was composed of four parts: infrared controller, infrared, experimental wall, and data acquisition instrument. The heat of infrared controlled by an infrared controller at a certain constant temperature was used to heat the surface of the experimental wall, and a data acquisition instrument was able to collect the temperatures with the variations of time via thermocouples, which were the data required by the simulations. The temperatures of the surface opposite the heated surface could also be determined by the average of the four temperatures measured by the thermocouples arranged in the middle of four bricks at the second and third layers, respectively, which could be compared with the simulation results to verify the accuracy of the simulation process. In addition to the

charging process, the experiments at the discharging stage were conducted by turning off the infrared and recording the temperature variations in the process of natural cooling to room temperature. In addition, the experimental wall and infrared were positioned in parallel, and the distance between them was maintained at a constant 30 cm.

2.3. Grid Independence

The verification of grid independence for the model was carried out on the phase change wall with EHS/5 wt.% BN as the PCMs. The mesh images of walls with different grid amounts of 159,016, 48,082, and 18,762 are shown in Figure 4a–c, respectively, and the corresponding simulation results are compared in Figure 4d, which suggest that there was almost no difference among the three profiles. Therefore, the wall model with 48,082 grid amounts was used for the later simulation, and the time step was set as 1 s, considering the balance between the calculational time and accuracy.

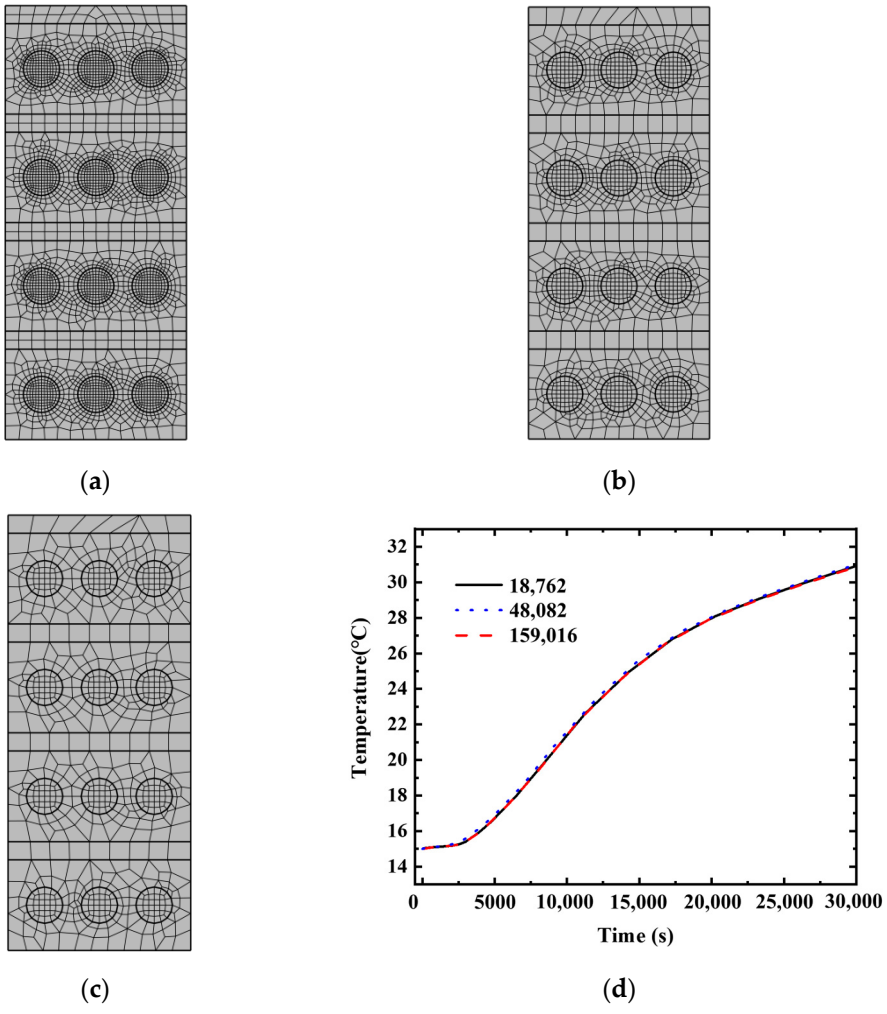

Figure 4. Schematic diagram of phase change wall after grid division with different grid quantities: (**a**) 159,016 grid quantity; (**b**) 48,082 grid quantity; and (**c**) 18,762 grid quantity. (**d**) Simulation results at the heating temperature of 50 °C under different grid quantities.

3. Simulation Results

Both the simulations and the experiments were carried out under the three heating temperatures of 50 °C, 55 °C, and 60 °C at two stages of charging and discharging, and the obtained results were presented and analyzed as follows.

3.1. Pure Brick Wall

The accuracy of the simulation can be determined by comparing the temperatures of the internal surface of the wall obtained from the experimental and the simulation data, and the time duration of the temperature within the thermal comfort range was used as the quantitative evaluation index. The typical curves of temperature variation at the internal surface of the pure brick wall corresponding to the simulation and experimental results [32] at both the charging and discharging stages are compared in Figure 5(a-I,a-II). The specific values of time duration within the thermal comfort range under the different heating temperatures of 50 °C, 55 °C, and 60 °C are summarized in Table 3. It can be concluded that there exists good agreement between the experimental and simulation results. The deviations of the time duration in the charging and discharging processes were approximately 10% and 7%, respectively, which were likely to be attributed to the influence of the fluctuation of the environmental temperature during the experiments and the existence of the thermal contact resistance between the bricks and the cement.

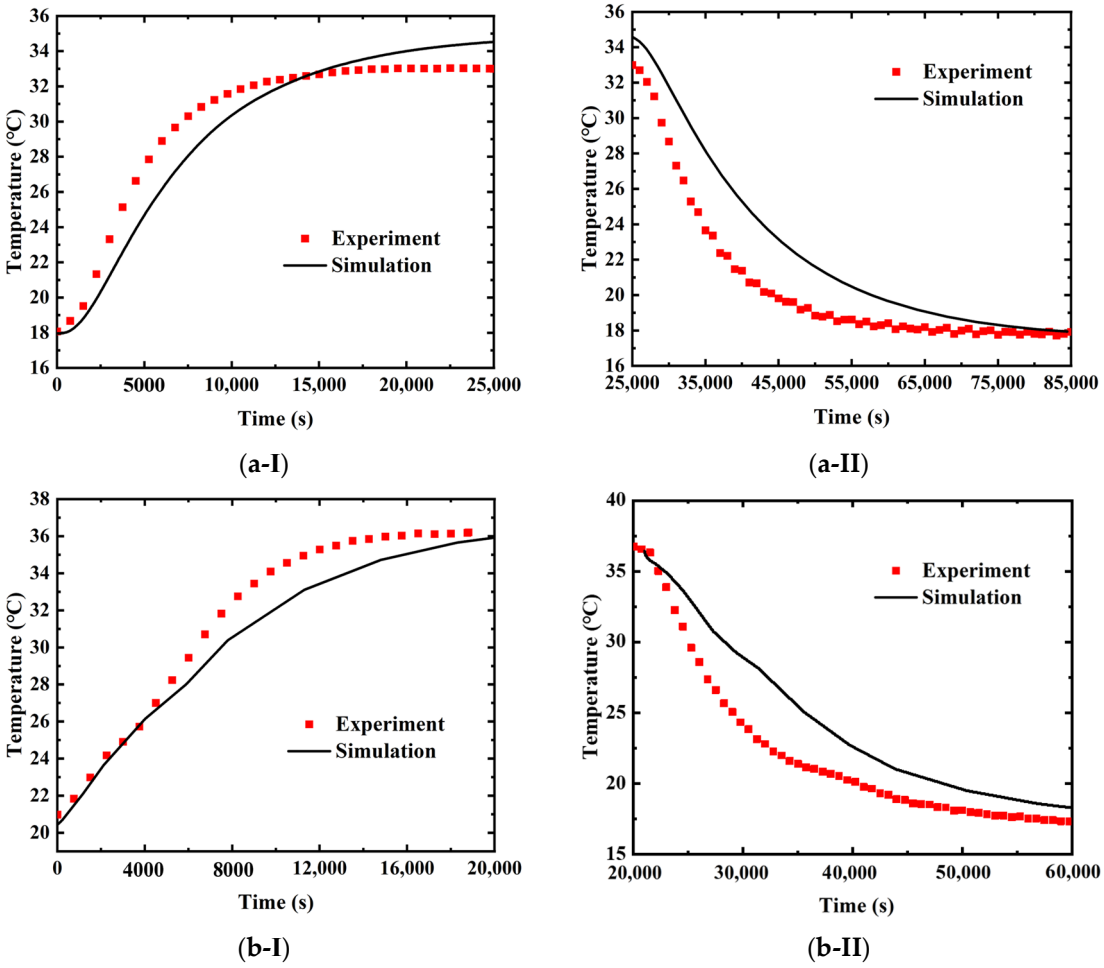

Figure 5. Comparisons between simulation and experimental results of pure brick wall and phase change walls with EHS/5 wt.% BN/7.5 wt.% EG as PCMs: (**a-I**) charging stage at 55 °C of pure brick wall; (**a-II**) discharging stage of pure bricks wall; (**b-I**) charging stage at 60 °C of phase change wall; (**b-II**) discharging stage of phase change wall.

Table 3. Time duration within thermal comfort temperature range at different heating temperatures of pure brick wall.

Stage	Heating Temperature	Time Duration within the Thermal Comfort Temperature Range (s) (Simulation Results)
Charging	50 °C	6383
	55 °C	3499
	60 °C	3011
Discharging	50 °C	7562
	55 °C	8220
	60 °C	7404

3.2. Phase Change Walls

Both the phase change walls with EHS/5 wt.% BN and EHS/5 wt.% BN/7.5 wt.% EG as the PCMs, respectively, were simulated and investigated under the heating temperatures of 50 °C, 55 °C, and 60 °C. Considering the phase change wall with EHS/5 wt.% BN/7.5 wt.% EG as PCMs at 60 °C as an example, the comparative results at the charging and discharging stages are presented in Figure 5(b-I,b-II). In the charging stage, the rate of temperature rise turned out to be smaller, approximately 26 °C, which could be explained by the phase change behavior of the PCMs, which absorbed abundant heat and led to the temperature increasing more slowly. In the discharging stage, the existence of a supercooling phenomenon of the PCMs caused the evidently reduced temperature drop rate to appear at approximately 22 °C, lower than the melting temperature of 26 °C. In addition, the values of the specific heat capacity used in the charging process were applied to simulate the discharging process due to the difficulty in obtaining the correct specific heat capacity of the PCMs in the solidification process by DSC, which also brought about the deviation between the results of the experiments and the simulations due to the subcooling degree. The specific values of time duration within the thermal comfort temperature range for the two types of phase change walls are shown in Table 4.

Table 4. Time duration within thermal comfort temperature range at different heating temperatures of phase change walls.

PCM Filled into Bricks	Heating Temperature	Time Duration within the Thermal Comfort Temperature Range (s) (Simulation Results)
EHS/5 wt.% BN	50 °C	12,093
	55 °C	7002
	60 °C	5021
EHS/5 wt.% BN/7.5 wt.% EG	50 °C	6722
	55 °C	4734
	60 °C	4102

3.3. Comparisons between the Pure Brick Wall and Phase Change Walls

The temperature nephograms at 2000 s, 4000 s, 6000 s, and 8000 s of the three types of walls, including the pure brick wall, phase change wall with EHS/5 wt.% BN/7.5 wt.% EG as the PCMs, and another phase change wall with EHS/5 wt.% BN as the PCMs, and cross sections of the walls from the external to the internal sides during the charging process under the heating temperature of 50 °C are shown in Figure 6, Figure 7 and Figure 8, respectively. The temperature range of color legends for all the temperature nephograms was set from 15 °C to 60 °C for the convenience of mutual comparison. It can be seen intuitively that the overall temperatures of the walls gradually increased due to the heat transferred from the outside to the inside, and the pure brick wall corresponded to the highest internal surface temperature and the largest temperature rise rate within 8000 s due

to the poor heat storage performance compared with the phase change walls. In addition, the phase change wall with EHS/5 wt.% BN as the PCMs had the lowest internal surface temperature due to the optimal heat storage effects brought about by the largest specific heat capacity during the phase change process. Similar heat transfer characteristics for the three types of walls appeared in the temperature nephograms of the cross section of the walls in terms of the rate of the temperature rise. Therefore, it was concluded that the phase change walls made contributions to delaying the heat transferred from the external to the internal sides, and the brick wall filled with EHS/5 wt.% BN presented an advantage in terms of thermoregulation performance.

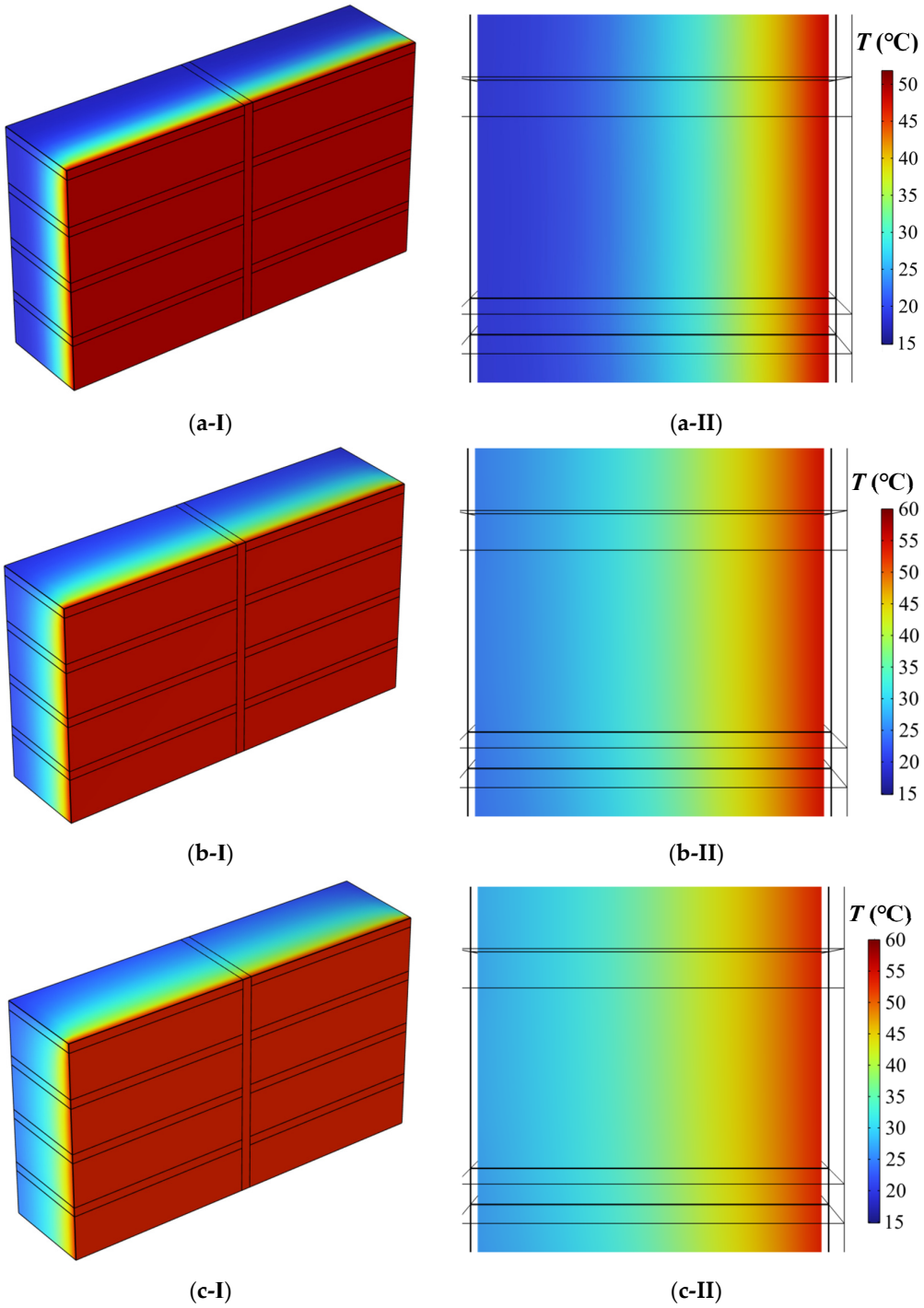

Figure 6. *Cont.*

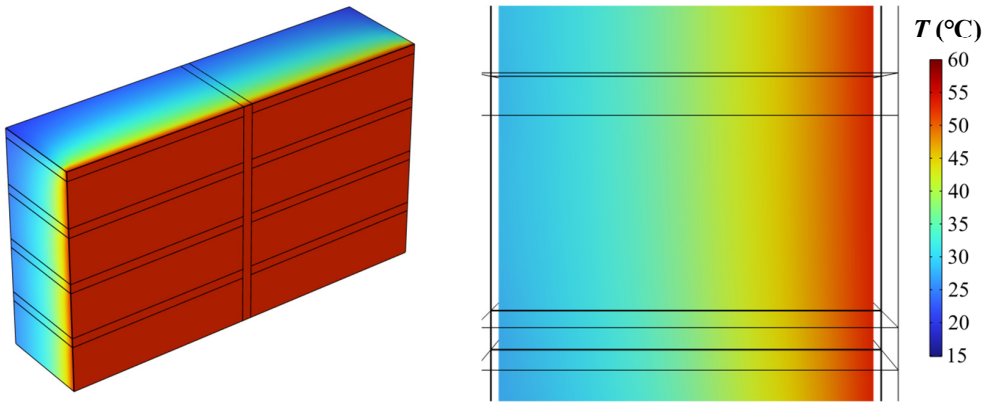

(**d-I**) (**d-II**)

Figure 6. Temperature contours of pure brick wall at different times: (**a-I**) overall cloud map at 2000 s; (**a-II**) internal cross section at 2000 s; (**b-I**) overall cloud map at 4000 s; (**b-II**) internal cross section at 4000 s; (**c-I**) overall cloud map at 6000 s; (**c-II**) internal cross section at 6000 s; (**d-I**) overall cloud map at 8000 s; (**d-II**) internal cross section at 8000 s.

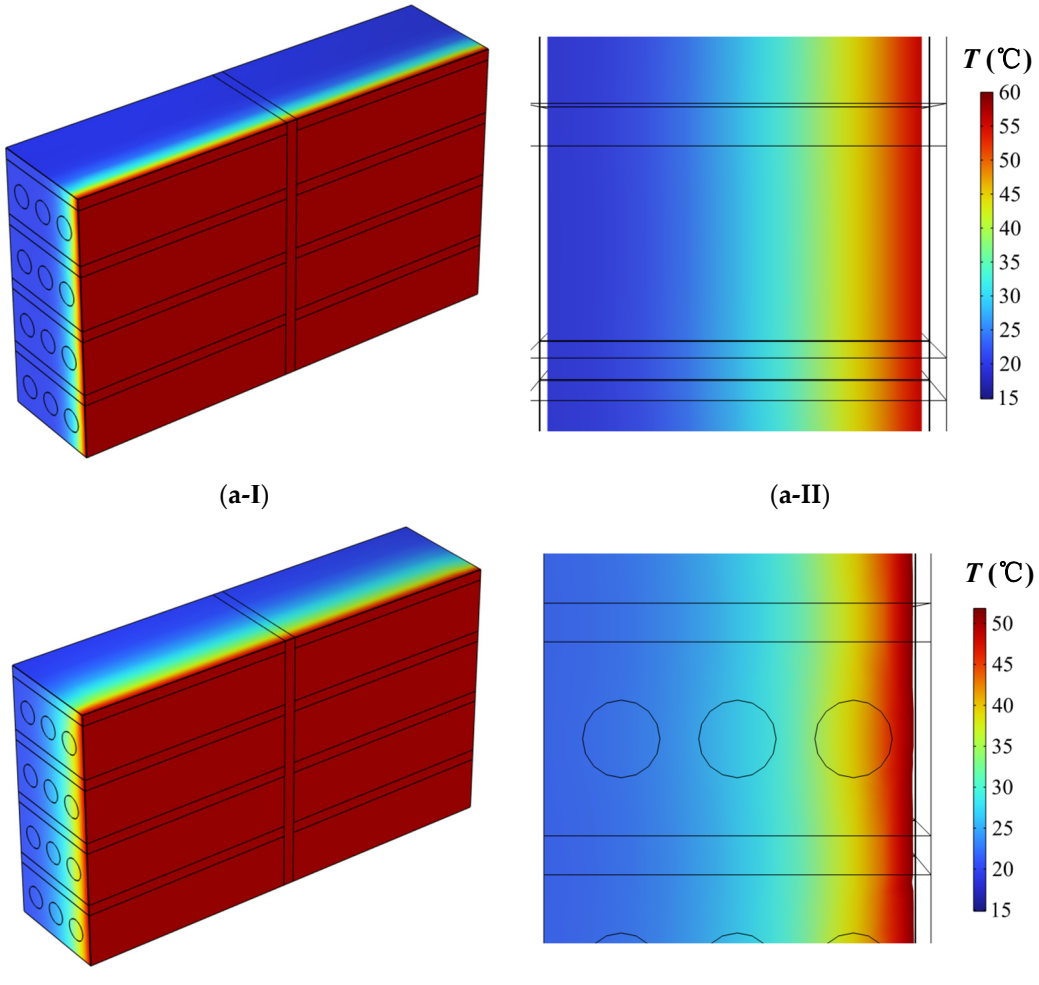

(**a-I**) (**a-II**)

(**b-I**) (**b-II**)

Figure 7. *Cont.*

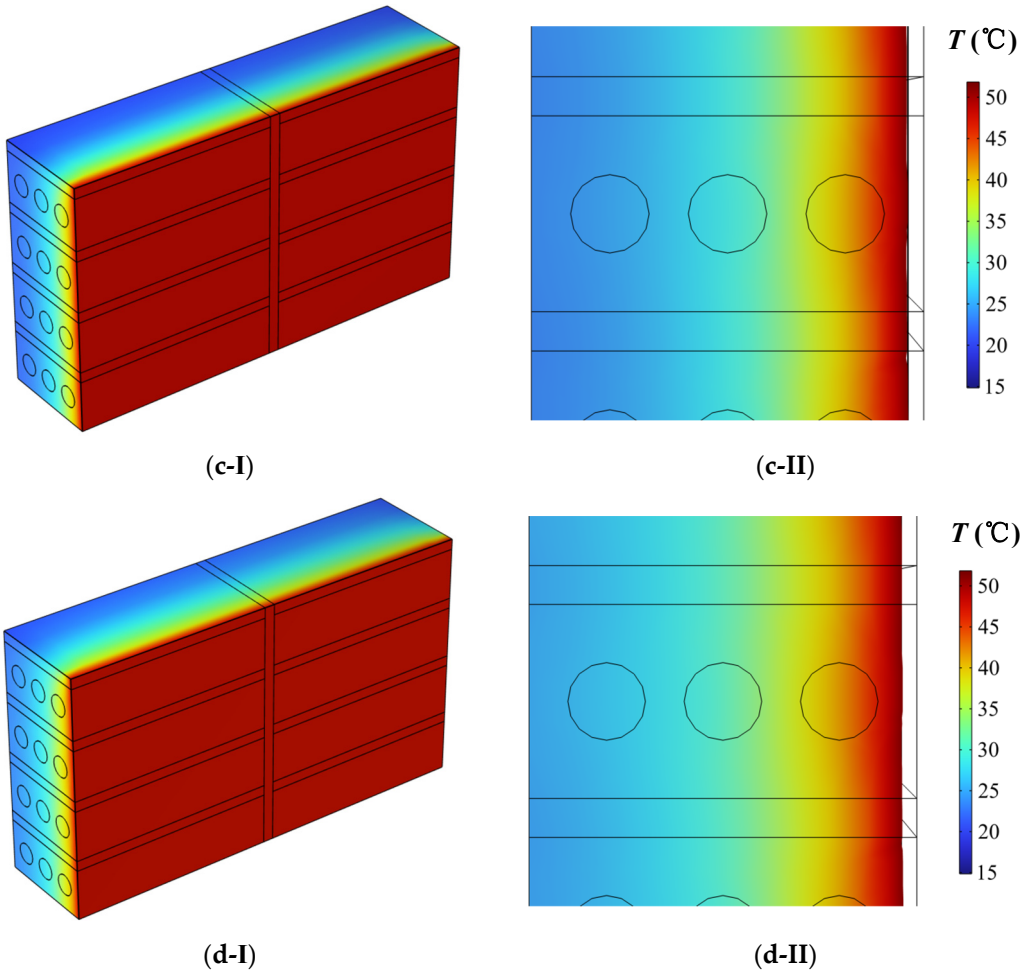

Figure 7. Temperature contours of phase change wall filled with EHS/5 wt.% BN/7.5 wt.% EG: (**a-I**) overall cloud map at 2000 s; (**a-II**) internal cross section at 2000 s; (**b-I**) overall cloud map at 4000 s; (**b-II**) internal cross section at 4000 s; (**c-I**) overall cloud map at 6000 s; (**c-II**) internal cross section at 6000 s; (**d-I**) overall cloud map at 8000 s; (**d-II**) internal cross section at 8000 s.

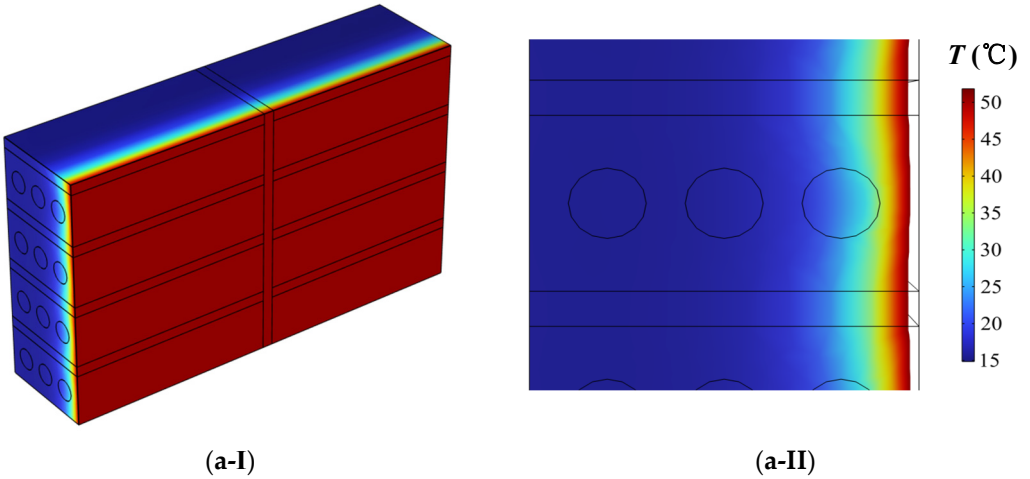

Figure 8. *Cont.*

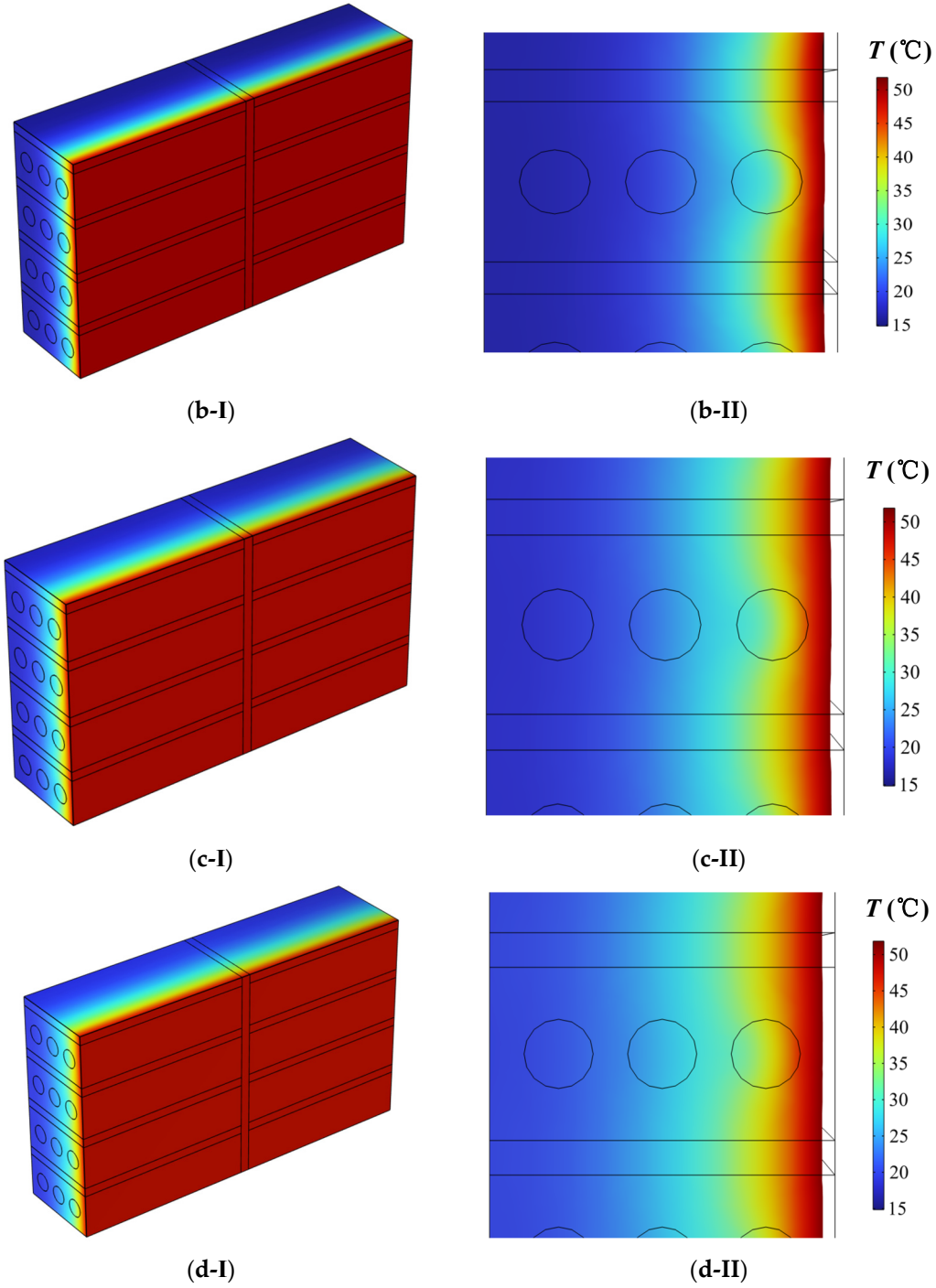

Figure 8. Temperature contours of phase change wall filled with EHS/5 wt.% BN: (**a-I**) overall cloud map at 2000 s; (**a-II**) internal cross section at 2000 s; (**b-I**) overall cloud map at 4000 s; (**b-II**) internal cross section at 4000 s; (**c-I**) overall cloud map at 6000 s; (**c-II**) internal cross section at 6000 s; (**d-I**) overall cloud map at 8000 s; (**d-II**) internal cross section at 8000 s.

4. Machine Learning

The application of machine learning to the studies of phase change walls has outstanding advantages in terms of prediction ability and low costs, which, therefore, can be used in combination with the experiments and simulations. Currently, the research method of machine learning are involved mainly with the random forest method [21], logistic regression method [33], artificial neural network method [34], and Bayesian learning method [35]. In the present study, the BP neural network method with the prediction ability for nonlinear

system was adopted to conduct machine learning on the thermoregulation effects of the phase change walls and to make predictions. In addition, it was found that the EHS/5 wt.% BN/7.5 wt.% EG as the PCMs had the best leakage prevention in a preliminary study [32]. The content of machine learning was focused on the variations of the time duration of the temperature at the internal side within the thermal comfort range during the charging process for the phase change wall with EHS/5 wt.% BN/7.5 wt.% EG as the PCMs under different environmental conditions to reveal the thermal response characteristics.

4.1. The Introduction to the BP Neural Network

The BP neural network relies on the information connection and delivery layer by layer to process abundant data by imitating the animal neural structure [19]. The training samples were first input into the input layer and then transmitted from the hidden layer to the output layer. Finally, the output results could be obtained via signal transformation.

The schematic diagram of the topological structure of the BP neural network is presented in Figure 9. The calculation expression of the output is $y = \Sigma\omega_i x_i - \theta_i$, where x_i is the input value; ω_i denotes the synaptic weight of the neuron; and θ_i refers to the threshold of a certain layer. Additionally, when the neuron outputs the objects, an appropriate activation function is required to be employed due to the nonlinearity of the data, and the frequently used activation functions are introduced as follows: Softmax function, Tansig function, Relu function, and Sigmoid function. Generally speaking, the Tansig function is adopted at the hidden layer, while the Sigmoid function is used at the output layer to address the classification issues; however, this is not fixed, and it is necessary to make some adjustments based on the results of machine learning. In the present study, the Tansig function was applied for each layer, and its expression is shown in Equation (5):

$$f(z) = \tan sig(z) = \frac{\exp(z) - \exp(-z)}{\exp(z) + \exp(-z)} \quad (5)$$

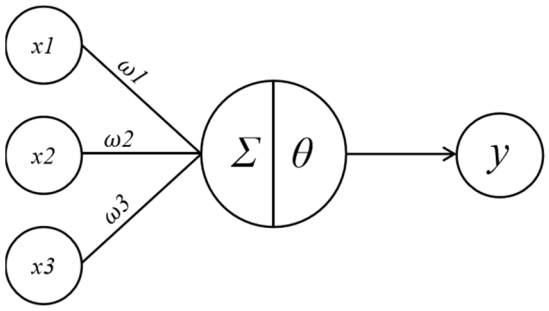

Figure 9. Schematic diagram of the topological structure of BP neural network.

In the training process of machine learning, the associated parameters, such as the numbers of hidden layers and nodes, the learning rate, and the momentum factor, are required to be set and then modified based on the training results, especially for the number of hidden nodes. Having fewer hidden nodes tends to cause a decrease in the machine learning ability of the entire neural network; therefore, the performance processing of the data and the prediction accuracy would be lowered. Moreover, hidden nodes in large quantities also reduce the learning efficiency due to the increase in the complexity of the model, which definitely consumes a longer learning time and introduces the problem of overfitting. Thus, the number of hidden nodes can be gradually increased from a small level in a small-scale neural network. Figure 10 shows the specific logical procedures of the BP neural network in this work. Before training, firstly, the input and output parameters were defined; the former denotes the independent variable, while the latter denotes the dependent variable influenced by the input parameters. In addition, 70% of the data collected were used as the training set, and the remainder of the data were evenly divided into two parts to serve as the verification and test sets, respectively. Moreover, the

training parameters should be adjusted multiple times and then determined. In terms of the stopping criteria of the training process of machine learning, the associated requirements should be satisfied and are described as follows:

(1) The maximum training times serve as the first judgment basis. When the training times reach the maximum value, the training process can be stopped. Otherwise, the training accuracy error must be inspected.

(2) The training accuracy error is the next level judgment parameter. If the training results meet the requirement of deviation accuracy, the training process can be regarded as completed. Otherwise, the training must continue to proceed.

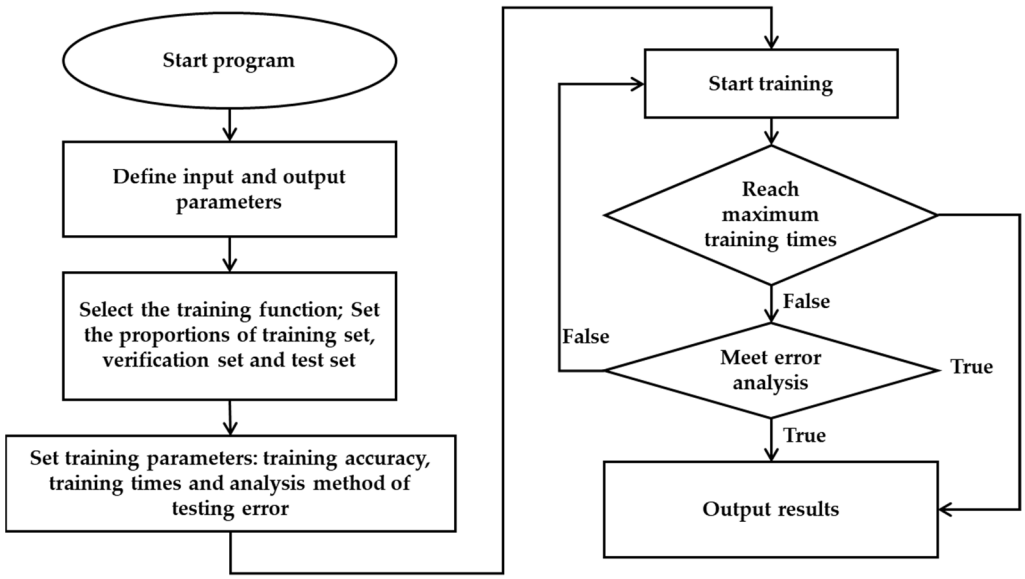

Figure 10. Logical structure diagram of BP neural network program.

4.2. Parameters Determination in the BP Neural Network

In the BP neural network, the raw data were divided into training, testing, and verification sets in the random form, and the Bayesian regularization function was used for training on the neural network. The training set provides the raw data for training in machine learning, and the verification set can be used to check the learning effects after several iteration processes. When the accuracy of the learning model is found to have little increase, it is necessary to modify the associated parameters required to avoid the appearance of this issue after the learning process is finished. The data of the test set are not covered by machine learning and, thus, can be employed to measure the learning effects of the final model. Generally, including more data in the training set tends to produce better training effects. The effects of machine learning in this study would decrease if the raw data were involved only in the results from the experiments [32]. Therefore, simulations were conducted to apply the corresponding results to further enlarge the amount of raw data. It was demonstrated that there existed a good agreement between the experiment and the simulation results; hence, the wall model could be used to make simulations to enrich the training set. In this work, the ambient temperature and heating temperature were defined as input parameters, the specific scope of which are shown in Table 5. The ambient temperature varied within the range of 18~24 °C; here, 2 °C was a changing internal, while the heating temperature varied from 36 °C to 72 °C, and the corresponding changing internal was set as 3 °C. In addition, the time duration of the temperature at the internal side within the thermal comfort range of 22~28 °C was the output parameter. Figure 11 shows the variations of the thermal comfort duration at the ambient temperature of 18 °C as the heating temperature increased from 45 °C to 72 °C based on the simulation results, and it was revealed that the thermal comfort duration decreased to 3787 s when the heating temperature reached 72 °C.

Table 5. Input parameters settings.

Input Parameter	Range	Unit
Ambient temperature	(18, 2, 24)	°C
Heating temperature	(36, 3, 72)	°C

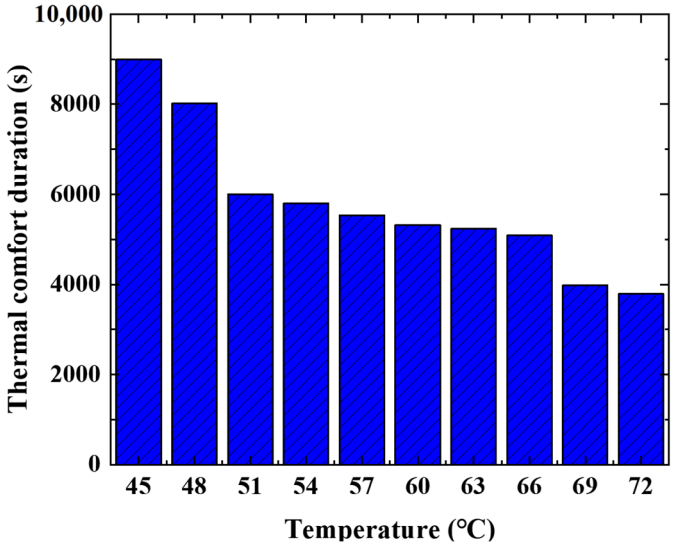

Figure 11. Time duration within the thermal comfort temperature range.

The determined values of the critical parameters of the BP neural network are summarized in Table 6. In consideration of the single change trend between the input and output parameters after the adjustments, two hidden layers were arranged, and the corresponding numbers of neural units were set to 30 and 40. Additionally, the maximum number of iterations, the learning rate, and the momentum factor were determined as 50, 0.01, and 0.9, respectively. Additionally, the quality of the training results was evaluated by the mean squared error, and the deviation of the training accuracy was set to 0.25% to enhance its accuracy. The entire training process underwent multiple stages, including the input layer, hidden layer, and output layer, with the intention of obtaining the optimization results.

Table 6. Key parameters of BP neural network.

Key Parameter	Value
Number of hidden layers	2
Numbers of neural units of hidden layers	30, 40
Activation function of hidden layers	Tansig
Maximum number of iterations	50
Learning rate	0.01
Momentum factor	0.9
Training accuracy	0.0025
Error analysis	MSE

4.3. Machine Learning Results Based on the BP Neural Network

The entire training process underwent 50 iterations. The training accuracy could be enhanced after each iteration, and the final accuracy met the set requirement. The data fitting effects of the training and test sets at 25 and 50 iterations exhibited a difference. Specifically, the distribution of the output data was relatively scattered after 25 iterations, and the fitting effects failed to reach the required training accuracy, producing the fitting correlation coefficients of training and test results of only 0.96388 and 0.7922, respectively; therefore, the training process was required to proceed. By contrast, both fitting correlation

coefficients of the training and test results exceeded 0.99 after 50 iterations, which are clearly shown in Figure 12. In addition, the training accuracy error was only 0.000211, which is lower than 0.0025. Therefore, it can be concluded that the training accuracy of machine learning achieved the expected effects, and, thus, the training process could be completed.

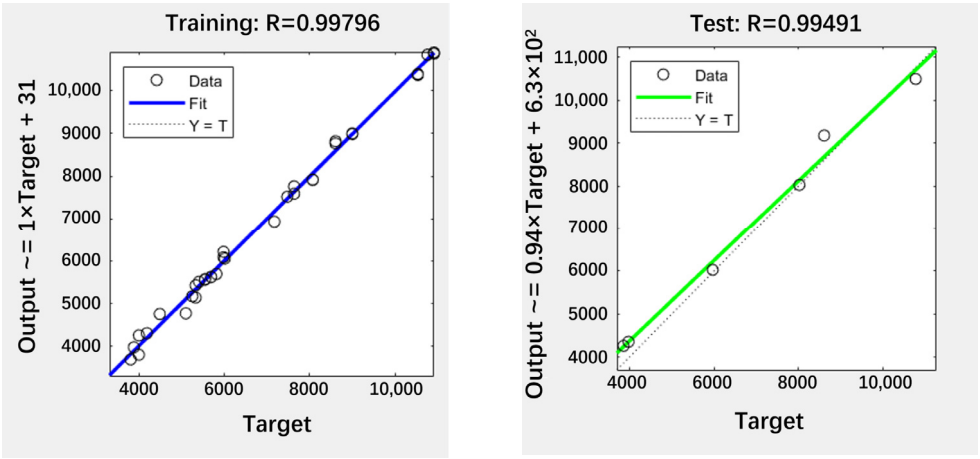

(**a**) (**b**)

Figure 12. Training results of BP neural network after 50 iterations: (**a**) training set and (**b**) test set.

In addition to the studies on the fitting effects of the training and test data, the accuracy of the BP neural network after training was further verified based on the difference between the learning results and the simulation data. Ten sets of data from the raw data were input again into the model after the training process to obtain the specific deviation, and the comparative results are shown in Figure 13. It was suggested that most deviations were approximately 2%, and the maximum one corresponded to 69 °C, which equaled 4.9%, which was lower than 5%. On the whole, there was no appearance of overfitting or underfitting issues, and the BP neural network presented good machine learning effects in terms of the thermoregulation performance of a single wall, making it suitable to use in further predictions studies.

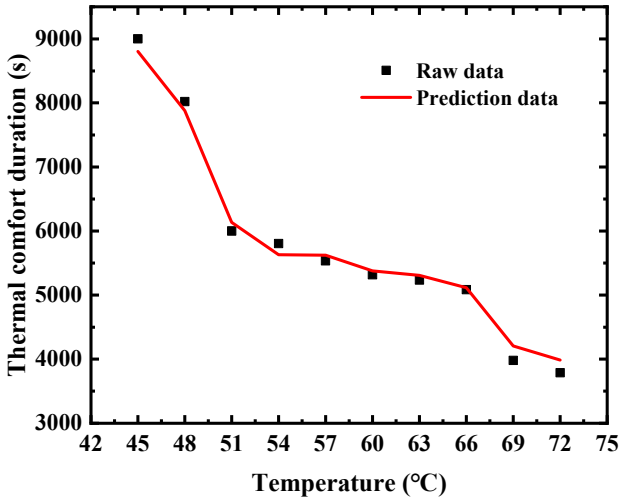

Figure 13. Comparisons between machine learning results and raw data.

The prediction effects of the BP neural network for the phase change walls need to be evaluated by the input of the unknown parameters that were excluded in the raw data. In view of the ambient temperature of the raw data within the range of 18~24 °C, the ambient temperature of the input data to be predicted was input as 18 °C or 24 °C, and another

input parameter, namely the heating temperature, was randomly determined, as shown in Table 7. Simultaneously, simulations were conducted at the same conditions. It can be seen that the prediction results were close to the simulation data under different conditions, and only a relatively large deviation appeared at ambient temperature of 24 °C and the heating temperature of 58.5 °C; however, this was still less than 3.5%. Thus, it can be concluded that the BP neural network had the ability to accurately predict the thermoregulation effects of the phase change walls. In addition, machine learning exhibited the strength of having a low time cost. The entire training process of the BP neural network was completed in only 12 s, and the machine learning model after verification could take several seconds to make predictions. By contrast, 2~3 days would be consumed to simulate the thermoregulation performance of the phase change wall under a certain ambient temperature and heating temperature. Therefore, the application of machine learning to the studies of phase change walls presented outstanding merits in terms of research cost and efficiency.

Table 7. Value comparison between prediction and simulation results.

Ambient Temperature (°C)	Heating Temperature (°C)	Simulation Results (s)	Prediction Results (s)
18	52.5	5862	5706
18	58.5	5394	5507
18	70.5	3863	4007
24	52.5	9724	9593
24	58.5	7324	7810
24	70.5	5793	5880

5. Conclusions

In the present study, the application of PCMs of hydrate salts with high charging/discharging efficiencies, low costs, and great potential to the building envelope was studied to discuss the thermoregulation performance of the phase change walls at the inner faces under different environmental conditions via simulations and machine learning. The thermal response characteristics of the phase change walls provided valuable information and a basis for the practical usage of PCMs in the building envelope in terms of the improvement of indoor thermal comfort. The obtained conclusions are as follows:

(1) The pure brick wall corresponded to the largest rate of temperature rise in the charging process. By contrast, the phase change walls could evidently decay the heat transferred from the external to the internal sides. The brick wall filled with EHS/5 wt.% BN/7.5 wt.% EG presented worse storage effects compared with that filled with EHS/5 wt.% BN due to its lower latent heat value and larger thermal conductivity. However, EHS/5 wt.% BN/7.5 wt.% EG had a better leakage performance and, thus, had greater prospects for practical application in the building envelope.

(2) As the heating temperature increased, the extension effects of thermal comfort duration brought by the PCMs were weakened due to the increase in heat transfer, e.g., the time duration for EHS/5 wt.% BN at 50 °C and 60 °C were 12,093 s and 5021 s, respectively.

(3) The BP neural network was adopted to conduct machine learning on the thermoregulation performance of the phase change wall, which suggested that the learning deviation between the raw data and the test results obtained from the BP neutral network was within 5%. It was also found that the BP neural network after being well trained could accurately predict the time duration of the temperature at the internal side maintained within the thermal comfort since the deviation could be restricted to within 3.5%, which suggested that machine learning had great prospects in the heat storage of buildings.

(4) In the future, in addition to the exploration of PCMs with greater thermal properties and cyclic stability, the application studies of phase change walls in different building types and more actual building situations, such as the various sources of humans and

equipment being considered, deserve to be carried out. Moreover, unified standards for the evaluation of energy consumption and economic benefits are expected to be established for the determination of reasonable applications of using PCMs in the building envelope.

Author Contributions: Conceptualization, X.X. and H.J.; methodology, X.X. and H.J.; software, H.J.; validation, H.J. and Q.H.; formal analysis, Q.H.; investigation, H.J.; resources, X.X.; data curation, X.X. and A.B.; writing—original draft preparation, Q.H.; writing—review and editing, X.X. and Q.H.; visualization, X.X. and H.J.; supervision, X.X.; project administration, X.X.; funding acquisition, X.X. and Y.W. All authors have read and agreed to the published version of the manuscript.

Funding: This research was funded by the Shanghai Pujiang Program, grant number 20PJ1400200; Yunnan Provincial Rural Energy Engineering Key Laboratory, grant number 2022KF001; the Fundamental Research Funds for the Central Universities of China, grant number 2232021D-11.

Data Availability Statement: Not applicable.

Acknowledgments: The authors would like to thank Thermal Energy Storage and Management Laboratory of Donghua University for the validated experiments.

Conflicts of Interest: The authors declare no conflict of interest.

References

1. Zhan, H.; Mahyuddin, N.; Sulaiman, R.; Khayatian, F. Phase change material (PCM) integrations into buildings in hot climates with simulation access for energy performance and thermal comfort: A review. *Constr. Build. Mater.* **2023**, *397*, 132312. [CrossRef]
2. Javidan, M.; Asgari, M.; Gholinia, M.; Nozari, M.; Asgari, A.; Ganji, D.D. Thermal energy storage inside the chamber with a brick wall using the phase change process of paraffinic materials: A numerical simulation. *Theor. Appl. Mech. Lett.* **2022**, *12*, 100329. [CrossRef]
3. Li, M.; Yan, D.; Shi, J. Multi-scale simulation study on the heat transfer characteristics of phase-change walls. *Energy* **2022**, *259*, 124896. [CrossRef]
4. Ye, R.; Lin, W.; Fang, X.; Zhang, Z. A numerical study of building integrated with $CaCl_2 \cdot 6H_2O$/expanded graphite composite phase change material. *Appl. Therm. Eng.* **2017**, *126*, 480–488. [CrossRef]
5. Derradji, L.; Errebai, F.B.; Amara, M. Effect of PCM in improving the thermal comfort in buildings. *Energy Procedia* **2017**, *107*, 157–161. [CrossRef]
6. Charvátová, H.; Procházka, A.; Zálešák, M. Computer simulation of passive cooling of wooden house covered by phase change material. *Energies* **2020**, *13*, 6065. [CrossRef]
7. Ye, R.; Huang, R.; Fang, X.; Zhang, Z. Simulative optimization on energy saving performance of phase change panels with different phase transition temperatures. *Sustain. Cities Soc.* **2020**, *52*, 101833. [CrossRef]
8. Zhu, N.; Li, S.; Hu, P.; Lei, F.; Deng, R. Numerical investigations on performance of phase change material Trombe wall in building. *Energy* **2019**, *187*, 116057. [CrossRef]
9. Rehman, A.U.; Sheikh, S.R.; Kausar, Z.; McCormack, S.J. Numerical simulation of a novel dual layered phase change material brick wall for human comfort in hot and cold climatic conditions. *Energies* **2021**, *14*, 4032. [CrossRef]
10. Gopinath, G.R.; Muthuvel, S.; Dinesh, N.; Karthikeyan, G.; Haashim, A. Thermal performance of phase change material embedded in building Wall–a numerical analysis. *Mater. Today Proc.* **2022**, *66*, 712–716. [CrossRef]
11. Kant, K.; Shukla, A.; Sharma, A. Numerical simulation of building wall incorporating phase change material for cooling load reduction. *Energy Clim. Chang.* **2020**, *1*, 100008. [CrossRef]
12. Govindasamy, D.; Panwar, V. Effect of variation in thickness of phase change material on temperature across the composite building wall. *Mater. Today Proc.* **2021**, *46*, 10221–10226. [CrossRef]
13. Rai, A.C. Energy performance of phase change materials integrated into brick masonry walls for cooling load management in residential buildings. *Build. Environ.* **2021**, *199*, 107930. [CrossRef]
14. Zhang, G.; Xiao, N.; Wang, B.; Razaqpur, A.G. Thermal performance of a novel building wall incorporating a dynamic phase change material layer for efficient utilization of passive solar energy. *Constr. Build. Mater.* **2022**, *317*, 126017. [CrossRef]
15. Mi, X.; Liu, R.; Cui, H.; Memon, S.A.; Xing, F.; Lo, Y. Energy and economic analysis of building integrated with PCM in different cities of China. *Appl. Energy* **2016**, *175*, 324–336. [CrossRef]
16. Qu, Y.; Zhou, D.; Xue, F.; Cui, L. Multi-factor analysis on thermal comfort and energy saving potential for PCM-integrated buildings in summer. *Energy Build.* **2021**, *241*, 110966. [CrossRef]
17. Wang, P.; Liu, Z.; Xi, S.; Zhang, Y.; Zhang, L. Experiment and numerical simulation of an adaptive building roof combining variable transparency shape-stabilized PCM. *Energy Build.* **2022**, *263*, 112030. [CrossRef]
18. Abd El-Raheim, D.; Mohamed, A.; Fatouh, M.; Abou-Ziyan, H. Comfort and economic aspects of phase change materials integrated with heavy-structure buildings in hot climates. *Appl. Therm. Eng.* **2022**, *213*, 118785. [CrossRef]

19. Stergiou, K.; Ntakolia, C.; Varytis, P.; Koumoulos, E.; Karlsson, P.; Moustakidis, S. Enhancing property prediction and process optimization in building materials through machine learning: A review. *Comput. Mater. Sci.* **2023**, *220*, 112031. [CrossRef]
20. Zhang, L.; Wen, J.; Li, Y.; Chen, J.; Ye, Y.; Fu, Y.; Livingood, W. A review of machine learning in building load prediction. *Appl. Energy* **2021**, *285*, 116452. [CrossRef]
21. Hussien, A.; Khan, W.; Hussain, A.; Liatsis, P.; Al-Shamma'a, A.; Al-Jumeily, D. Predicting energy performances of buildings' envelope wall materials via the random forest algorithm. *J. Build. Eng.* **2023**, *69*, 106263. [CrossRef]
22. Bacher, P.; Madsen, H.; Nielsen, H.A.; Perers, B. Short-term heat load forecasting for single family houses. *Energy Build.* **2013**, *65*, 101–112. [CrossRef]
23. Idowu, S.; Saguna, S.; Åhlund, C.; Schelén, O. Applied machine learning: Forecasting heat load in dis trict heating system. *Energy Build.* **2016**, *133*, 478–488. [CrossRef]
24. Al-Shammari, E.T.; Keivani, A.; Shamshirband, S.; Mostafaeipour, A.; Yee, P.L.; Petković, D.; Ch, S. Prediction of heat load in district heating systems by Support Vector Machine with Firefly searching algorithm. *Energy* **2016**, *95*, 266–273. [CrossRef]
25. Jovanović, R.Ž.; Sretenović, A.A.; Živković, B.D. Ensemble of various neural networks for prediction of heating energy consumption. *Energy Build.* **2015**, *94*, 189–199. [CrossRef]
26. Xiao, Z.; Fan, C.; Yuan, J.; Xu, X.; Gang, W. Comparison between artificial neural network and random forest for effective disaggregation of building cooling load. *Case Stud. Therm. Eng.* **2021**, *28*, 101589. [CrossRef]
27. Ahmad, M.W.; Mourshed, M.; Rezgui, Y. Trees vs Neurons: Comparison between random forest and ANN for high-resolution prediction of building energy consumption. *Energy Build.* **2017**, *147*, 77–89. [CrossRef]
28. Bhamare, D.K.; Saikia, P.; Rathod, M.K.; Rakshit, D.; Banerjee, J. A machine learning and deep learning based approach to predict the thermal performance of phase change material integrated building envelope. *Build. Environ.* **2021**, *199*, 107927. [CrossRef]
29. Alnaqi, A.A.; Alsarraf, J.; Al-Rashed, A.A.A.A. Transient numerical study on injecting PCM in buildings along with extra comfort ventilation: Use of artificial neural network to decline energy utilization. *Eng. Anal. Bound. Elem.* **2022**, *143*, 559–567. [CrossRef]
30. Urresti, A.; Campos-Celador, A.; Sala, J.M. Dynamic neural networks to analyze the behavior of phase change materials embedded in building envelopes. *Appl. Therm. Eng.* **2019**, *158*, 113783. [CrossRef]
31. Su, Z.-Y.; Li, J. Comparative study on thermal comfort of different patterns of commercial complex in summer in Guangzhou. *Urban. Archit.* **2020**, *17*, 120–125. [CrossRef]
32. Xiao, X.; Jiao, H.-S.; Hu, Q.; Li, M.; Wang, Y.F. Experimental study on supercooling retrieval of hydrated salts with nano additives and its application in building envelope. In Proceedings of the Third International Conference on Chinese Energy and Built Environment, Shanghai, China, 29 July–1 August 2023.
33. Yamaguchi, Y.; Miyachi, Y.; Shimoda, Y. Stock modelling of HVAC systems in Japanese commercial building sector using logistic regression. *Energy Build.* **2017**, *152*, 458–471. [CrossRef]
34. Kubwimana, B.; Najafi, H. A novel approach for optimizing building energy models using machine learning algorithms. *Energies* **2023**, *16*, 1033. [CrossRef]
35. Tan, J.; Maleki, P.; An, L.; Luigi, M.D.; Villa, U.; Zhou, C.; Ren, S.; Faghihi, D. A predictive multiphase model of silica aerogels for building envelope insulations. *Comput. Mech.* **2022**, *69*, 1457–1479. [CrossRef]